Exceptional and Anisotropic Transport Properties of Photocarriers in Black Phosphorus

Jiaqi He,[†,‡] Dawei He,[†] Yongsheng Wang,[*,†] Qiannan Cui,[‡] Matthew Z. Bellus,[‡] Hsin-Ying Chiu,[‡] and Hui Zhao[*,‡]

[†]Key Laboratory of Luminescence and Optical Information, Ministry of Education, Institute of Optoelectronic Technology, Beijing Jiaotong University, Beijing 100044, China and [‡]Department of Physics and Astronomy, The University of Kansas, Lawrence, Kansas 66045, United States

ABSTRACT One key challenge in developing postsilicon electronic technology is to find ultrathin channel materials with high charge mobilities and sizable energy band gaps. Graphene can offer extremely high charge mobilities; however, the lack of a band gap presents a significant barrier. Transition metal dichalcogenides possess sizable and thickness-tunable band gaps; however, their charge mobilities are relatively low. Here we show that black phosphorus has room-temperature charge mobilities on the order of 10^4 cm^2 V^{-1} s^{-1}, which are about 1 order of magnitude larger than silicon. We also demonstrate strong anisotropic transport in black phosphorus, where the mobilities along the armchair direction are about 1 order of magnitude larger than in the zigzag direction. A photocarrier lifetime as long as 100 ps is also determined. These results illustrate that black phosphorus is a promising candidate for future electronic and optoelectronic applications.

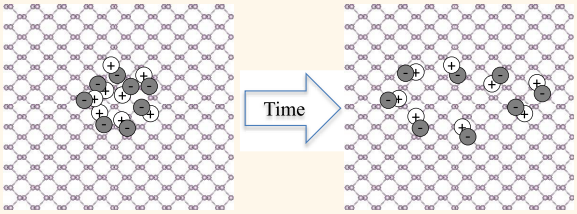

KEYWORDS: black phosphorus · charge transport · transient absorption · carrier lifetime

The rapid development of silicon-based integrated circuit technology over the past several decades relied on shrinking the channel length of the transistors. This approach is facing a severe challenge posted by several fundamental limits. Hence, recently, significant efforts have been devoted to finding new materials for postsilicon electronic technology. One promising candidate, graphene, has shown room-temperature charge mobilities 2 orders of magnitude higher than silicon.[1,2] However, the lack of a band gap limits its application as a channel material in logic devices. Since 2012, transition metal dichalcogenides, such as MoS_2, have been extensively studied.[3] These monolayer semiconductors have sizable band gaps[4,5] and possess several novel optical and spin/valley-related properties.[6] However, their charge mobilities are still lower than desired.

Since 2014, two-dimensional black phosphorus (BP), also known as phosphorene, has emerged as a new promising material to provide both a sizable band gap and high charge mobilities. Few-layer and monolayer BP can be fabricated from bulk crystals by mechanical[7] and liquid[8] exfoliation. Although bulk BP has a relatively small band gap[9] of 0.3 eV, several studies[7,10−12] have shown that the band gap of BP thin films depends strongly on the thickness when approaching the monolayer limit—a feature similar to other two-dimensional materials: Charge transfer characteristics of field-effect transistors indicated a band gap of 1.0 eV in monolayers;[10] while a 2.0 eV monolayer band gap was suggested by a scanning tunneling microscopy measurement on the surface of bulk BP.[11] Photoluminescence peaks from excitons were observed at 1.45 eV in monolayer BP[7] and evolve from 1.3 to 0.9 eV when the number of atomic layers are changed from two to five.[12] Without knowing the exciton binding energies, these numbers give the lower limits of the band gap. Although more studies are still necessary to precisely determine the band gaps, the fact that few-layer BP possesses band gaps large enough for logic applications has been established. On transport properties, theoretical studies indicated that monolayer and few-layer BP possess high room-temperature mobilities[13] on the order of 10^4 cm^2 V^{-1} s^{-1} and can

* Address correspondence to yshwang@bjtu.edu.cn, huizhao@ku.edu.

Received for review April 8, 2015 and accepted May 11, 2015.

Published online May 11, 2015
10.1021/acsnano.5b02104

outperform silicon and MoS_2 in ballistic devices.[14,15] Experimentally, field-effect transistors of multilayer BP have been fabricated.[7,16−20] These transistors can have a long operation lifetime once passivated by top Al_2O_3 layers,[21,22] and can operate at the GHz regime.[23] In optoelectronic applications, high photoresponsitivity[24] and broadband response to both visible and infrared radiations[25] have been demonstrated in BP. Utilizing the ambipolar transport behavior, the photovoltaic effect was demonstrated in few-layer BP in a local-gate p−n junction configuration.[26]

Here we report experimental observations of exceptional transport performance of multilayer BP and its high in-plane anisotropy. By resolving spatiotemporal dynamics of photocarriers that are instantaneously injected by a tightly focused ultrashort laser pulse, we obtain room-temperature diffusion coefficients of 1300 and 80 $cm^2\ s^{-1}$ for photocarriers moving along the armchair and zigzag directions, respectively. These values correspond to ambipolar mobilities on the order of 50 000 and 3000 $cm^2\ V^{-1}\ s^{-1}$, respectively. We also find that the photocarrier lifetime in multilayer BP is about 100 ps. These results provide fundamental parameters of BP and illustrate its great promise for electronic and optoelectronic applications.

RESULTS AND DISCUSSION

A bulk BP crystal has orthorhombic symmetry, as illustrated in Figure 1a, where single layers of phosphorus atoms are stacked by van der Waals force. In each layer, phosphorus atoms form a puckered honeycomb lattice, as shown in Figure 1b. Figure 1c shows the sample used in this study. It contains a 16 nm BP flake exfoliated from a bulk crystal (see Method). To prevent direct exposure to air, the flake is partially covered by a 4 nm boron nitride (BN) layer.

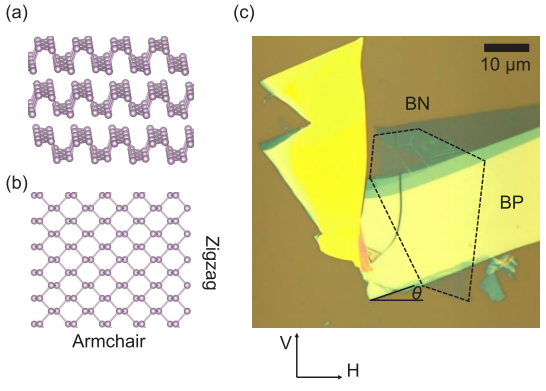

Figure 1. Lattice structure of black phosphorus and sample image. (a) Lattice structure of multilayer black phosphorus. (b) Top view of a monolayer black phosphorus, with armchair and zigzag directions. (c) Optical image of the sample studied. The black phosphorus (BP) flake of 16 nm thick is partially covered by a 4 nm boron nitride (BN) flake, indicated by the dashed line. The horizontal (H) and vertical (V) directions in the laboratory frame are labeled. The angle θ is between H and the long edge of the flake.

All the measurements were performed in ambient condition. No sample degradation was observed during the entire course of the study.

In our transient absorption measurements, a 730 nm and 100 fs laser pulse with a peak fluence of 10 $\mu J\ cm^{-2}$ injects electron−hole pairs in the sample. The pulse is linearly polarized along the long edge of the flake, as shown in Figure 1c. The dynamics of the injected photocarriers are monitored by measuring the differential reflection of a 810 nm probe pulse that is polarized along the direction perpendicular to the pump polarization. The differential reflection ($\Delta R/R_0$) is defined as the pump-induced relative change of the probe reflection (see Methods). As shown in Figure 2a, the differential reflection signal reaches a peak near zero probe delay. After a transient process of about 20 ps, the signal decays exponentially (red line), with a time constant of 100 ± 5 ps. We attribute this to the carrier lifetime in BP. By repeating the measurement

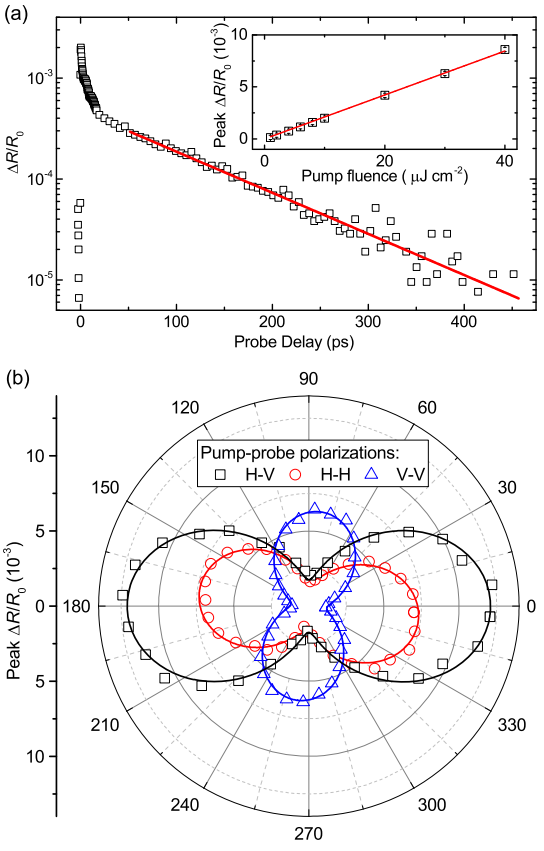

Figure 2. Time-resolved differential reflection signal from black phosphorus and its angular dependence. (a) Differential reflection ($\Delta R/R_0$) measured with a 730 nm pump and a 810 nm probe pulses. The red line indicates a single-exponential fit with a time constant of 100 ± 5 ps. The inset shows a linear relation between the peak signal and the pump fluence. (b) The peak differential reflection signal as a function of θ, the angle between the long edge of the flake and the horizontal direction in the laboratory frame. The black squares, red circles, and blue triangles are measured with the pump−probe polarization configurations of horizontal−vertical (H−V), horizontal−horizontal (H−H), and vertical−vertical (V−V), respectively.

with different values of the pump fluence (and hence different densities of the injected carriers), we confirm that the peak differential reflection signal is proportional to the pump fluence, as shown in the inset of Figure 2a.

The lattice structure of BP shown in Figure 1b dictates that its in-plane properties are anisotropic, since the effective masses of the electrons and holes depend strongly on the crystalline direction.[13,27−29] Indeed, the anisotropic optical responses of BP have been predicted[13,30] and experimentally confirmed by polarization-dependent Raman scattering[12,17] and absorption.[17] To study the anisotropic transient absorption of BP, we measure the differential reflection signal with different pump−probe polarization configurations as we rotate the sample with respect to the polarization directions. The squares, circles, and triangles in Figure 2b show the peak signal of differential reflection as a function of the angle (θ) between the long edge of the flake and the horizontal direction in the laboratory frame [Figure 1c], with the pump−probe polarizations of horizontal−vertical (H−V), H−H, and V−V, respectively. Pronounced anisotropy is clearly seen in all the configurations. The solid lines in Figure 2b are fits to the data by $A\cos^2(\theta + \theta_0) + B$, with $\theta_0 = 0°$, $-8°$, and $82°$ for H−V, H−H, and V−V configurations, respectively.

The angular dependence of the differential reflection signal shown in Figure 2b can be induced by two factors: the pump absorption and the probe detection efficiency.

First, because of the different effective masses along the armchair and zigzag directions, the absorption coefficients are expected to be different when the pump pulses are polarized along different directions. Hence, as the sample is rotated with respect to the pump polarization, the pump injects different carrier densities, which results in an angular dependent signal level. This effect can be quantified by comparing the peak differential reflection signals at $\theta = 0$ in H−V (12×10^{-3}) and V−V (1.3×10^{-3}) configurations: The only difference between these two measurements is that the pump polarization is either parallel or perpendicular to the long edge of the flake. On the basis of the reported optical conductivity tensor of BP obtained from Kubo formula, the maximal absorption should occur when the polarization is along the armchair direction.[30] Therefore, we identify the long edge of the flake as the armchair direction. It is interesting to note that even with the pump photon energy much larger than the band gap, the absorption coefficient for light polarized along the armchair direction is still about 10 times larger than the zigzag direction.

The second factor inducing the observed anisotropic differential reflection response is the dependence of the probing efficiency on the probe polarization. To quantify this effect, we compare the signals at $\theta = 0$ in H−V (12×10^{-3}) and H−H (7.2×10^{-3}) configurations, which show that the probe polarized along the zigzag direction is a factor of 1.7 more efficient in sensing the carriers than that polarized along the armchair direction. Unlike the absorption coefficient, which is determined by the imaginary part of the optical conductivity, the differential reflection originates from the pump-induced changes in both the real and the imaginary parts of the optical conductivity in a rather complex manner. In particular, since the probe photon energy is much larger than the band gap, the differential optical conductivity at the probe wavelength is likely induced by a combination of screening and phase-space state filling effects of the carriers.[31] Further theoretical studies are necessary to relate the measured anisotropy to the differential optical conductivity tensor. Here, we just note that the anisotropic effect of the probe is smaller than that of the pump and plays a minor role in determining the angular dependence of the differential reflection. This is also consistent with the observation that the angular dependence of H−V is aligned with H−H, instead of V−V. The small rotation of the H−H pattern with respect to H−V (8°) is caused by the compromise of anisotropic pump and probe effects. The V−V pattern is rotated by 90° from H−H, which confirms that the angular dependence observed is not from any artifacts of the experimental system.

The results shown in Figure 2b not only reveal the anisotropic optical response of BP, they also allow us to identify the crystalline direction of the sample, and hence facilitate measurements of photocarrier transport along different directions. In the spatially resolved differential reflection measurements, the tightly focused 730 nm pump injects photocarriers with a Gaussian spatial profile of about $w = 2.4$ μm in full width at half-maximum. Once injected, the photocarriers diffuse in each atomic layer, driven by the in-plane density gradient. Hence, the spatial density profile expands. This diffusion process is monitored by measuring the differential reflection of the probe as a function of the probe delay and probe position.

First, we study diffusion of the photocarriers along the long edge direction of the flake, which is identified as the armchair direction according to Figure 2b. In this measurement, both pump and probe polarizations are along the armchair direction, and the probe spot is scanned along the same direction. Figure 3a shows the differential reflection signal as a function of the probe delay and probe spot position with respect to the pump spot. At each probe delay, the profile has a Gaussian shape. Figure 3b shows three examples of these profiles at probe delays of 2 (squares), 10 (circles), and 20 ps (triangles), respectively, along with the corresponding Gaussian fits (solid lines). From each fit, we obtain the width (full width at half-maximum) of the profile. The squared width is plotted in Figure 3c as a function of the probe delay.

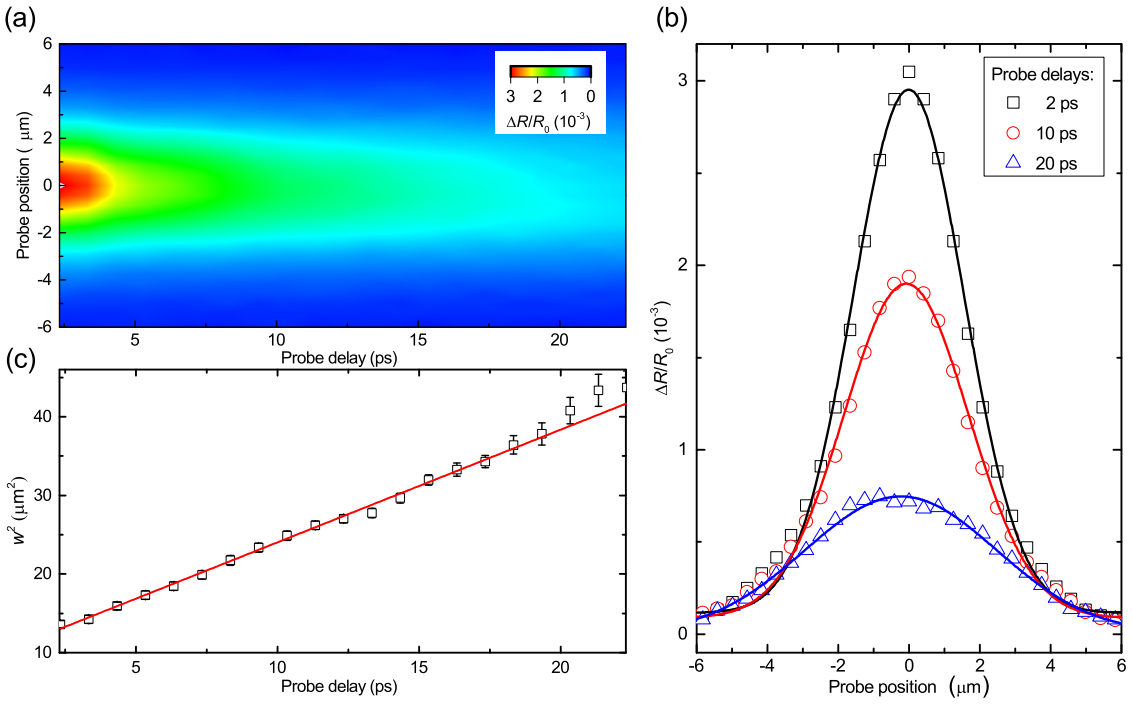

Figure 3. Photocarrier diffusion along the armchair direction of black phosphorus. (a) Differential reflection as a function of the probe delay and probe position obtained by scanning the probe spot with respect to the pump spot along the armchair direction for each probe delay. (b) Examples of the spatial profiles of the differential reflection signal, obtained with probe delays of 2 (squares), 10 (circles), and 20 ps (triangles), respectively. The solid lines are Gaussian fits. (c) The squared width as a function of the probe delay. The solid line is a linear fit that gives a diffusion coefficient of 1300 ± 30 cm^2 s^{-1}.

According to the diffusion model,[32] the profile of the carrier density remains in its Gaussian shape during the diffusion, as confirmed in Figure 3b. The width of the profile evolves as $w^2(t) = w^2(t_0) + 16\ \ln(2)D(t - t_0)$, where t_0 is an arbitrarily chosen initial time, and D is the diffusion coefficient. Such a linear expansion of the area covered by the photocarriers is confirmed by the linear fit to the data shown in Figure 3c (red line). From the slope, we obtain a diffusion coefficient of 1300 ± 30 cm^2 s^{-1}.

The above analysis to deduce the diffusion coefficient requires that the recombination of the photocarriers is independent of the carrier density. Otherwise, carriers at different locations within the profile would decay at different rates, which could change the shape and size of the profile even without carrier diffusion. To rule out such an artifact, we measure the decay of the differential reflection signal as a function of the carrier density by varying the pump fluence. We find that during the range of the probe delay used for the diffusion measurement, the decay is independent of the carrier density (see Supporting Information, Figure S2). This ensures that the recombination of carriers only changes the height of the profile, but not the shape or width, and hence the broadening observed in Figure 3 is due to the diffusion.

Next, we rotate the sample by 90° and repeat the measurement under otherwise the same conditions. Now the polarizations and the scan directions are all along the zigzag direction. The results are presented in Figure 4, in the same fashion as Figure 3. Clearly, the diffusion is much slower along the zigzag direction. From a linear fit, shown as the solid line in Figure 4c, we obtain a diffusion coefficient of 80 ± 5 cm^2 s^{-1}, which is about a factor of 16 smaller than along the armchair direction.

The spatially resolved measurements also help us understand the nonexponential decay shown in Figure 2a, with a fast transient process of about 20 ps during which the signal dropped by about a factor of 4. As a rough estimation from Figures 3c and 4c, the area of the profile increases by more than a factor of 2 in this time range. Hence, the peak of the profile should decrease by the same factor because of the diffusion along. On the other hand, at later probe delays, the diffusion makes a smaller contribution to the decay of the signal since the profile is already significantly broadened. This is confirmed by the single-exponential decay as indicated by the red line in Figure 2a and validates the attribution of the 100 ps time constant to the carrier lifetime. By using the diffusion coefficients and the lifetime (τ), we obtain the diffusion lengths $[(D\tau)^{1/2}]$ of about 4 and 1 μm along the armchair and zigzag directions, respectively.

The noninvasive and all-optical measurement of spatiotemporal dynamics of photocarriers in BP reveals its exceptional and highly anisotropic transport properties, which show the great potential of this material for electronic and optoelectronic applications. The measured diffusion coefficient can be used to deduce

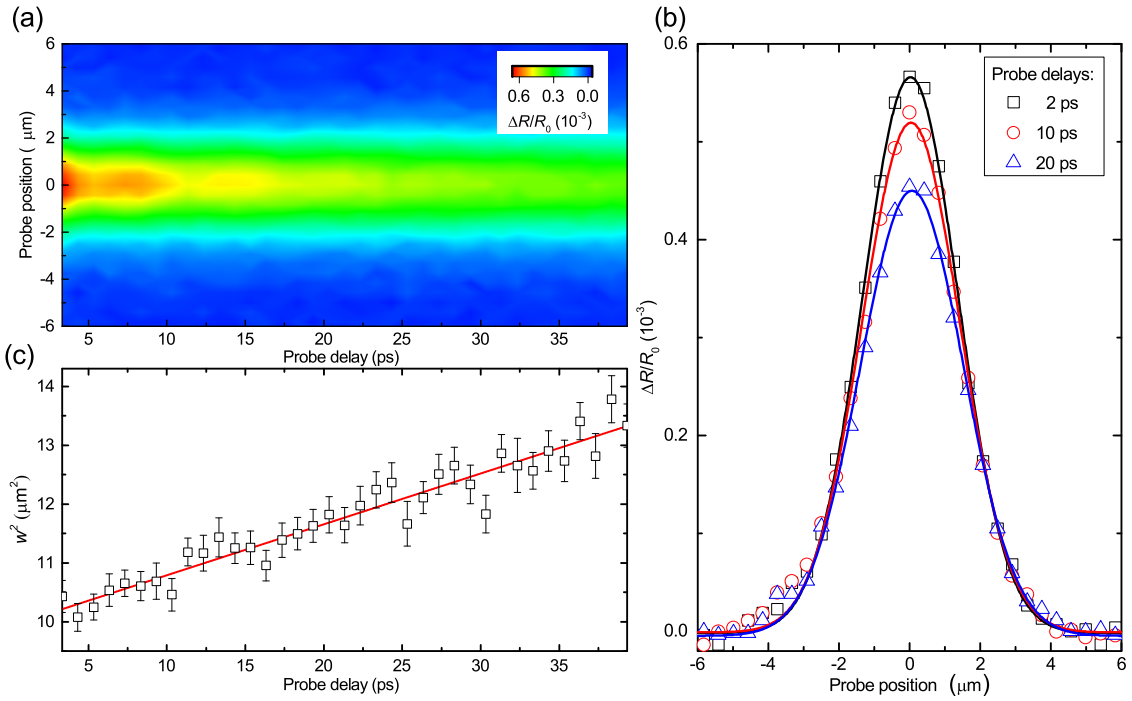

Figure 4. Photocarrier diffusion along the zigzag direction of black phosphorus. (a) Differential reflection as a function of the probe delay and probe position obtained by scanning the probe spot with respect to the pump spot along the zigzag direction for each probe delay. (b) Examples of the spatial profiles of the differential reflection signal, obtained with probe delays of 2 (squares), 10 (circles), and 20 ps (triangles), respectively. The solid lines are Gaussian fits. (c) The squared width as a function of the probe delay. The solid line is a linear fit that gives a diffusion coefficient of 80 ± 5 cm^2 s^{-1}.

the mobility by using the Einstein's relation, $\mu/e = D/k_BT$, where μ, e, k_B, and T are the mobility, elementary charge, Boltzmann constant, and temperature, respectively. We obtain mobilities of 50 000 ± 2000 and 3000 ± 200 cm^2 V^{-1} s^{-1} along armchair and zigzag directions, respectively.

In this diffusion process we studied, the electron−hole pairs injected by the pump are required to move as pairs by the charge neutrality:[33] Although the electrons and holes are unbound quasi-free particles, once an electron (hole) moves with respect to the pairing hole (electron), a space charge field is induced, which drags the hole (electron) to move with the electron (hole). Hence, the diffusion coefficients obtained are ambipolar diffusion coefficients, which are related to the diffusion coefficients of electrons and holes (D_e and D_h) by $D_a = 2D_eD_h/(D_e + D_h)$ for photocarriers.[33] In general, the ambipolar diffusion coefficient is controlled by the slower carriers. Hence, the ambipolar diffusion coefficient can be regarded as the lower limit of D_e and D_h. In BP, the effective masses of electrons and holes are within a factor of 2.[34] Hence, the ambipolar diffusion coefficient and ambipolar mobility provide satisfactory order-of-magnitude estimation of the diffusion coefficients and mobilities of both electrons and holes. In our discussion, we do not consider formation of excitons, which are unstable at room temperature with an exciton binding energy of 7.9 meV.[35] Hence, the photocarriers are mostly free electrons and holes, and neglecting excitonic effects does not influence the order-of-magnitude estimation of the charge mobilities.

Recently, high room-temperature charge mobilities on the order of 10^4 cm^2 V^{-1} s^{-1} in BP have been predicted theoretically.[13] The previously reported experimental values have yet to reach that level. For example, transistors of 10 nm BP flakes achieved mobilities in the range of 100−1000 cm^2 V^{-1} s^{-1} at room temperature,[7,16,17] and higher values were obtained at low temperatures.[18,19] A trilayer BP transistor demonstrated electron and hole mobilities of 38 and 172 cm^2 V^{-1} s^{-1}, respectively.[20] The electrical measurements may not reveal the intrinsic transport properties of the material since the transport can be limited by grain boundaries and by the quality of the electrodes. Indeed, a significant influence of the metal contact has been suggested.[36−38] On the other hand, the all-optical approach we used in this study does not involve device fabrication, and grain boundaries play a negligible role in the diffusion process. We find that our results are reasonably consistent with the theoretical predictions.[13]

The anisotropic transport property can be mainly attributed to the anisotropic effective masses of electrons and holes. The effective masses of electrons with wavevectors along the armchair and zigzag directions are $0.0825m_0$ and $1.027m_0$, respectively, where m_0 stands for the electron rest mass in vacuum. Hole effective masses are $0.0761m_0$ and $0.648m_0$ along the two directions, respectively.[34] The differences in

effective masses suggest that the mobilities along the armchair direction are about 1 order of magnitude larger than zigzag direction. Such a ratio is also predicted in monolayer and few-layer BP.[13,27] On the basis of our result, the mobility along the armchair direction is about 16 times larger than the zigzag direction, which is reasonably consistent with these predictions.

CONCLUSION

We studied photocarrier dynamics in multilayer black phosphorus by performing transient absorption measurements with high temporal and spatial resolutions. Strong anisotropic transient absorption responses were observed, which allow us to identify the armchair and zigzag directions. By following diffusion of photocarriers along these directions, we obtained diffusion coefficients of 1300 and 80 $cm^2\ s^{-1}$ and diffusion lengths of about 4 and 1 μm along the armchair and zigzag directions, respectively. These diffusion coefficients correspond to ambipolar mobilities on the order of 10^4 and 10^3 $cm^2\ V^{-1}\ s^{-1}$, respectively. These results illustrate that black phosphorus is a promising candidate for future electronic and optoelectronic applications.

METHODS

Thin films of BP were mechanically exfoliated from bulk crystals purchased from 2D Semiconductors. An adhesive tape is used to remove layers of BP from the crystal, which are then transferred to a SiO_2 (90 nm)/Si substrate. The identified flake is immediately covered by a thin boron nitride layer, which was prepared with the same procedure, in order to prevent its degradation in air. The sample used in this study is shown in Figure 1c. The thicknesses of the BP film and the boron nitride layer are determined to be 16 and 4 nm, respectively, according to atomic force microscopy measurements (Supporting Information, Figure S1).

The differential reflection setup utilizes an ultrafast laser system composed of a 2-W passively mode-locked Ti:sapphire oscillator and an optical parametric oscillator. The Ti:sapphire laser generates 100 fs pulse trains at 80 MHz, with a central wavelength of 810 nm. The majority of this beam is used to synchronically pump the optical parametric oscillator, which generates a signal output of 1460 nm. A second harmonic of this pulse at 730 nm is generated in a beta barium borate crystal, and is used as the pump. A small portion of the Ti:sapphire output is used as the probe.

In the differential reflection measurements, the pump and probe pulses are both focused to the sample surface to a spot size of about 2.4 μm in full width at half-maximum by using a microscope objective lens. The differential reflection of the probe is defined as the normalized change in the probe reflection induced by the pump, $\Delta R/R_0 \equiv (R - R_0)/R_0$. Here, R and R_0 are the reflection of the probe with the presence of the pump pulse or without it, respectively. The reflected probe is collimated by the same lens and is measured by a balanced detector. The output of the balanced detector is measured with a lock-in amplifier, with the intensity of the pump beam modulated at about 2 kHz with a mechanical chopper. The differential reflection is measured as a function of the probe delay, defined as the time delay of the probe pulse with respect to the pump pulse. This is achieved by controlling the length of the pump path with a linear motor stage. To spatially scan the probe spot across the pump spot, the incident angle of the probe beam to the objective lens is slightly changed from normal, achieved by a motorized mirror mount in the probe arm.

Conflict of Interest: The authors declare no competing financial interest.

Acknowledgment. The authors thank Jamie Wilt and Judy Wu for their help on the measurements of atomic force microscope. This material is based upon work supported by the National Science Foundation of USA (DMR-0954486, IIA-1430493), National Basic Research Program 973 of China (2011CB932700, 2011CB932703), Chinese Natural Science Fund Project (61335006, 61378073), Beijing Natural Science Fund Project (4132031), and Fundamental Research Funds for the Central Universities (2015YJS181).

Supporting Information Available: Sample characterization, influence of density on recombination. The Supporting Information is available free of charge on the ACS Publications website at DOI: 10.1021/acsnano.5b02104.

REFERENCES AND NOTES

1. Geim, A. K.; Novoselov, K. S. The Rise of Graphene. *Nat. Mater.* **2007**, *6*, 183–191.
2. Neto, A. H. C.; Guinea, F.; Peres, N. M. R.; Novoselov, K. S.; Geim, A. K. The Electronic Properties of Graphene. *Rev. Mod. Phys.* **2009**, *81*, 109–162.
3. Wang, Q. H.; Kalantar-Zadeh, K.; Kis, A.; Coleman, J. N.; Strano, M. S. Electronics and Optoelectronics of Two-Dimensional Transition Metal Dichalcogenides. *Nat. Nanotechnol.* **2012**, *7*, 699–712.
4. Mak, K. F.; Lee, C.; Hone, J.; Shan, J.; Heinz, T. F. Atomically Thin MoS_2: A New Direct-Gap Semiconductor. *Phys. Rev. Lett.* **2010**, *105*, 136805.
5. Splendiani, A.; Sun, L.; Zhang, Y.; Li, T.; Kim, J.; Chim, C. Y.; Galli, G.; Wang, F. Emerging Photoluminescence in Monolayer MoS_2. *Nano Lett.* **2010**, *10*, 1271–1275.
6. Xiao, D.; Liu, G. B.; Feng, W.; Xu, X.; Yao, W. Coupled Spin and Valley Physics in Monolayers of MoS_2 and Other Group-VI Dichalcogenides. *Phys. Rev. Lett.* **2012**, *108*, 196802.
7. Liu, H.; Neal, A. T.; Zhu, Z.; Luo, Z.; Xu, X.; Tomanek, D.; Ye, P. D. Phosphorene: An Unexplored 2D Semiconductor with a High Hole Mobility. *ACS Nano* **2014**, *8*, 4033–4041.
8. Brent, J. R.; Savjani, N.; Lewis, E. A.; Haigh, S. J.; Lewis, D. J.; O'Brien, P. Production of Few-Layer Phosphorene by Liquid Exfoliation of Black Phosphorus. *Chem. Commun.* **2014**, *50*, 13338–13341.
9. Warschauer, D. Electrical and Optical Properties of Crystalline Black Phosphorus. *J. Appl. Phys.* **1963**, *34*, 1853–1860.
10. Das, S.; Zhang, W.; Demarteau, M.; Hoffmann, A.; Dubey, M.; Roelofs, A. Tunable Transport Gap in Phosphorene. *Nano Lett.* **2014**, *14*, 5733–5739.
11. Liang, L.; Wang, J.; Lin, W.; Sumpter, B. G.; Meunier, V.; Pan, M. Electronic Bandgap and Edge Reconstruction in Phosphorene Materials. *Nano Lett.* **2014**, *14*, 6400–6406.
12. Zhang, S.; Yang, J.; Xu, R.; Wang, F.; Li, W.; Ghufran, M.; Zhang, Y. W.; Yu, Z.; Zhang, G.; Qin, Q.; *et al.* Extraordinary Photoluminescence and Strong Temperature/Angle-Dependent Raman Responses in Few-Layer Phosphorene. *ACS Nano* **2014**, *8*, 9590–9596.
13. Qiao, J.; Kong, X.; Hu, Z. X.; Yang, F.; Ji, W. High-Mobility Transport Anisotropy and Linear Dichroism in Few-Layer Black Phosphorus. *Nat. Commun.* **2014**, *5*, 4475.
14. Lam, K. T. Performance Limits Projection of Black Phosphorous Field-Effect Transistors. *IEEE Elec. Dev. Lett.* **2014**, *35*, 963–965.
15. Liu, F.; Wang, Y. J.; Liu, X. Y.; Wang, J.; Guo, H. Ballistic Transport in Monolayer Black Phosphorus Transistors. *IEEE T. Electron. Dev.* **2014**, *61*, 3871–3876.

16. Du, Y.; Liu, H.; Deng, Y.; Ye, P. D. Device Perspective for Black Phosphorus Field-Effect Transistors: Contact Resistance, Ambipolar Behavior, and Scaling. *ACS Nano* **2014**, *8*, 10035–10042.
17. Xia, F.; Wang, H.; Jia, Y. Rediscovering Black Phosphorus as an Anisotropic Layered Material for Optoelectronics and Electronics. *Nat. Commun.* **2014**, *5*, 4458.
18. Li, L.; Yu, Y.; Ye, G. J.; Ge, Q.; Ou, X.; Wu, H.; Feng, D.; Chen, X. H.; Zhang, Y. Black Phosphorus Field-Effect Transistors. *Nat. Nanotechnol.* **2014**, *9*, 372–377.
19. Liu, H.; Neal, A. T.; Si, M. W.; Du, Y. C.; Ye, P. D. The Effect of Dielectric Capping on Few-Layer Phosphorene Transistors: Tuning the Schottky Barrier Heights. *IEEE Electr. Dev. Lett.* **2014**, *35*, 795–797.
20. Das, S.; Demarteau, M.; Roelofs, A. Ambipolar Phosphorene Field Effect Transistor. *ACS Nano* **2014**, *8*, 11730–11738.
21. Na, J.; Lee, Y. T.; Lim, J. A.; do, K. H.; Kim, G. T.; Choi, W. K.; Song, Y. W. Few-Layer Black Phosphorus Field-Effect Transistors with Reduced Current Fluctuation. *ACS Nano* **2014**, *8*, 11753–11762.
22. Wood, J. D.; Wells, S. A.; Jariwala, D.; Chen, K. S.; Cho, E.; Sangwan, V. K.; Liu, X.; Lauhon, L. J.; Marks, T. J.; Hersam, M. C. Effective Passivation of Exfoliated Black Phosphorus Transistors against Ambient Degradation. *Nano Lett.* **2014**, *14*, 6964–6970.
23. Wang, H.; Wang, X.; Xia, F.; Wang, L.; Jiang, H.; Xia, Q.; Chin, M. L.; Dubey, M.; Han, S. J. Black Phosphorus Radio-Frequency Transistors. *Nano Lett.* **2014**, *14*, 6424–6429.
24. Buscema, M.; Groenendijk, D. J.; Blanter, S. I.; Steele, G. A.; van der Zant, H. S.; Castellanos-Gomez, A. Fast and Broadband Photoresponse of Few-Layer Black Phosphorus Field-Effect Transistors. *Nano Lett.* **2014**, *14*, 3347–3352.
25. Engel, M.; Steiner, M.; Avouris, P. Black Phosphorus Photodetector for Multispectral, High-Resolution Imaging. *Nano Lett.* **2014**, *14*, 6414–6417.
26. Buscema, M.; Groenendijk, D. J.; Steele, G. A.; van der Zant, H. S.; Castellanos-Gomez, A. Photovoltaic Effect in Few-Layer Black Phosphorus PN Junctions Defined by Local Electrostatic Gating. *Nat. Commun.* **2014**, *5*, 4651.
27. Ong, Z. Y.; Zhang, G.; Zhang, Y. W. Anisotropic Charged Impurity-Limited Carrier Mobility in Monolayer Phosphorene. *J. Appl. Phys.* **2014**, *116*, 214505.
28. Fei, R.; Yang, L. Strain-Engineering the Anisotropic Electrical Conductance of Few-Layer Black Phosphorus. *Nano Lett.* **2014**, *14*, 2884–2889.
29. Li, P.; Appelbaum, I. Electrons and Holes in Phosphorene. *Phys. Rev. B* **2014**, *90*, 115439.
30. Low, T.; Rodin, A. S.; Carvalho, A.; Jiang, Y. J.; Wang, H.; Xia, F. N.; Neto, A. H. C. Tunable Optical Properties of Multilayer Black Phosphorus Thin Films. *Phys. Rev. B* **2014**, *90*, 075434.
31. Schmitt-Rink, S.; Chemla, D. S.; Miller, D. A. B. Theory of Transient Excitonic Optical Nonlinearities in Semiconductor Quantum-Well Structures. *Phys. Rev. B* **1985**, *32*, 6601–6609.
32. Smith, L. M.; Wake, D. R.; Wolfe, J. P.; Levi, D.; Klein, M. V.; Klem, J.; Henderson, T.; Morkoç, H. Picosecond Imaging of Photoexcited Carriers in Quantum Wells: Anomalous Lateral Confinement at High Densities. *Phys. Rev. B* **1988**, *38*, 5788–5791.
33. Neamen, D. A. *Semiconductor Physics and Devices*; McGraw-Hill: Boston, 2002.
34. Morita, A.; Asahina, H.; Kaneta, C.; Sasaki, T. Anisotropic Mobility and Electron-Phonon Interaction in Black Phosphorus. *Proc. 17th Int. Conf. Phys. Semocond.* **1985**, 1320–1324.
35. Morita, A. Semiconducting Black Phosphorus. *Appl. Phys. A: Mater. Sci. Process.* **1986**, *39*, 227–242.
36. Gong, K.; Zhang, L.; Ji, W.; Guo, H. Electrical Contacts to Monolayer Black Phosphorus: A First-Principles Investigation. *Phys. Rev. B* **2014**, *90*, 125441.
37. Cai, Y.; Zhang, G.; Zhang, Y. W. Layer-Dependent Band Alignment and Work Function of Few-Layer Phosphorene. *Sci. Rep.* **2014**, *4*, 6677.
38. Wan, R.; Cao, X.; Guo, J. Simulation of Phosphorene Schottky-Barrier Transistors. *Appl. Phys. Lett.* **2014**, *105*, 163511.